applied sciences

MDPI

Article

High Repetition Rate and Coherent Free-Electron Laser Oscillator in the Tender X-ray Range Tailored for Linear Spectroscopy

Michele Opromolla [1,2,*], Alberto Bacci [2], Marcello Rossetti Conti [2], Andrea Renato Rossi [2], Giorgio Rossi [1], Luca Serafini [2], Alberto Tagliaferri [3] and Vittoria Petrillo [1,2]

[1] Dipartimento di Fisica, Universitá degli Studi di Milano, Via Celoria, 16 20133 Milano, Italy; giorgio.rossi2@unimi.it (G.R.); vittoria.petrillo@mi.infn.it (V.P.)
[2] INFN-Sezione di Milano, Via Celoria 16, 20133 Milano, Italy; alberto.bacci@mi.infn.it (A.B.); marcello.rossetticonti@mi.infn.it (M.R.C.); andrea.rossi@mi.infn.it (A.R.R.); luca.serafini@mi.infn.it (L.S.)
[3] Politecnico di Milano, P.zza Leonardo da Vinci, 20133 Milano, Italy; alberto.tagliaferri@polimi.it
* Correspondence: michele.opromolla@mi.infn.it

Abstract: Fine time-resolved analysis of matter—that is, spectroscopy and photon scattering—in the linear response regime requires fs-scale pulsed, high repetition rate, fully coherent X-ray sources. A seeded Free-Electron Laser, driven by a linac based on Super Conducting cavities, generating 10^8–10^{10} coherent photons at 2–5 keV with 0.2–1 MHz of repetition rate, can address this need. The scheme proposed is a Free-Electron Laser Oscillator at 3 keV, working with a cavity based on X-ray mirrors. The whole chain of the X-ray generation is here described by means of start-to-end simulations.

Keywords: free-electron lasers; X-rays; regenerative amplifiers

Citation: Opromolla, M.; Bacci, A.; Rossetti Conti, M.; Rossi, A.R.; Rossi, G.; Serafini, L.; Tagliaferri, A.; Petrillo, V. High Repetition Rate and Coherent Free-Electron Laser Oscillator in the Tender X-ray Range Tailored for Linear Spectroscopy. *Appl. Sci.* **2021**, *11*, 5892. https://doi.org/10.3390/app11135892

Academic Editor: Wilhelm Becker

Received: 14 May 2021
Accepted: 22 June 2021
Published: 24 June 2021

1. Introduction

Synchrotron radiation (SR) sources based on low-emittance electron storage rings, as well as Free Electron Lasers (FELs) driven by linear electron accelerators (Linacs), allow the fine analysis of matter, with applications extending from life sciences to material physics. Most FELs worldwide operate in the Self-Amplified Spontaneous Emission (SASE) mode [1–8], providing extremely brilliant and short pulses with more than 10^{12} photons per pulse, and shot-to-shot time and intensity jitters determined by the intrinsic fluctuations of the emission process. These Ultra-Violet (UV) or X-ray flashes are used to probe matter in highly excited states, to study nonlinear processes or to test before destroying individual objects such as macromolecules constituting proteins, thus replacing crystallography with single object imaging. In order to remain below the linear response threshold and to collect adequate statistics in a short time, spectroscopic probes, as well as pump–probe photoemission experiments in advanced atomic, molecular, nano- and solid- state physics, instead require ultra-short photon pulses (order 10 fs), MHz-class repetition rates and moderate fluxes of photons/pulse. Currently available FEL sources produce a number of photons per pulse exceeding by 2–4 orders of magnitude the linear response level: severe attenuation of the pulses, with a huge waste of energy, is therefore required in photoemission or X-ray absorption spectroscopy. The pulses' repetition rate is determined by the acceleration technology, and is much higher in Super-Conducting facilities, exceeding the 10–100 Hz range of Warm Linacs up to MHz-class [4,5]. Moreover, spectroscopic applications with X-ray FELs are severely limited by SASE fluctuations and full seeding, successfully conducted at FERMI (Free-Electron laser for Multidisciplinary Investigations) in the XUV-soft X-ray range [9], should ideally be extended to X-ray energies.

There is therefore a scientific need, and ample room, for a novel type of source that is able to provide 10 fs coherent pulses of 10^7–10^8 photons at 0.5–2 MHz in the tender X ray range, bridging the gap between the most advanced SR and the current FEL sources.

These demanding requests about structure, intensity, repetition rate, reduced jitters and true coherence of the pulses are addressed by conceiving a tailored seeded or self-seeded FEL driven by a linac based on Super Conducting cavities, providing 10^7–10^{10} coherent photons at 2–5 keV, at 1 MHz of repetition rate.

In the seeded amplifier FEL configuration, the pulses' stability and coherence is strongly increased by an external coherent source imprinting its temporal phase on the electron beam at the undulator entrance, thus enabling us to reach a high degree of temporal coherence within a short distance. The direct seeding [10] implementation is limited by the lack of high-power coherent seeds in the Vacuum-UV regime and below. High Gain Harmonic Generation (HGHG) multistage cascades [11], seeded with harmonics of an IR laser generated in crystals [11–13], were studied in the optical-UV range [14–16] and were demonstrated at FERMI up to a few nm wavelengths [9]. The implementation and reliability of this scheme in the tender/hard X-ray spectral range is highly demanding and has ye to be proven. In perspective, the X-ray range could be reached with the technique of the Echo Enabled Harmonic Generation (EEHG) [17–20], in which two coherent radiation pulses seed the electron beam in two sequential modulators interspersed by a strong dispersive section. Both cascaded schemes allow us to reach the boundary between Extreme Ultra-Violet and soft X-ray frequencies, and may be seeded by laser harmonics generated in gases or UV oscillators [21–24]. A major limit of all seeding schemes based on lasers is created by the achievable repetition rate, which is typically below tens of kHz, and their extension to higher repetition rates has so far only been studied theoretically [25–27].

The single spike SASE operation [28–30], as well as self-seeding processes [31,32], are able to achieve only partial longitudinal coherence. Another FEL configuration capable of producing stable radiation pulses is the FEL Oscillator (FELO), in which the radiation process builds up via multiple passes of a stable and high repetition rate pulse train of electron bunches through an undulator embedded in a low-loss optical cavity [23,33–37]. The lower gain required in such systems relaxes the requirements on peak current and electron beam quality. Thanks to the technological advancements in the field of optics and mirrors fabrication [38], FEL oscillators (XFELO) [37,39] and regenerative amplifiers (RAFEL) based on X-ray cavities [40–44] have been proposed as a direct source of coherent X-rays [36,37,40,45], or as seed for subsequent cascades [24,25,46]. However, limit cycle oscillations have been observed and studied in FELOs [47]: these fluctuations, depending on the cavity specifics and working point, can even be comparable to the fluctuations found in SASE FELs. Among all the methods for producing coherent X-ray radiation, we analyze here the case of a tender X-ray FEL Oscillator, driven by a moderate energy electron beam and based on a short period undulator. Diamond mirrors and beam splitters, foreseen at about 3 keV, constitute a ring cavity where the radiation pulses are synchronized with the electron bunches. In this paper, we show the operation of such a source. The electron beam is supposed to be generated by the accelerator of the MariX project (Multi-disciplinary Advanced Research Infrastructure for the generation and application of X-rays) [48], based on superconducting cavities and equipped with an arc compressor. The compact footprint (with a total dimension of less than 500 m) of the infrastructure and the contained costs should permit its construction in medium-sized research infrastructures or within university campuses. Hereafter, we will discuss the nominal parameters and start-to-end simulations of the system. Final comments will be presented in the conclusions.

2. Materials and Methods

Our analyses rely on the electron beam foreseen by the accelerator of the MariX project [48]. MariX is based on the innovative and compact design of a two-pass, two-way superconducting linear electron accelerator equipped with an arc compressor [49–51], to be operated in CW mode at 1 MHz. The characteristics of the electron beam, as evaluated after start-to-end simulations [52], are listed in Table 1. A short period, planar undulator can allow the production of radiation pulses in the desired wavelength range (5–2 Å, or

in energy 2–5 keV), starting from the moderate electron energy provided by the MariX accelerator (at a maximum of 3.8 GeV). From the resonance relation,

$$\lambda = \frac{\lambda_w}{2\gamma^2}(1 + a_w^2), \tag{1}$$

where $a_w = 0.657\lambda_w(\mathrm{cm})B(\mathrm{T})$ is the undulator parameter and γ the electron Lorentz factor for an electron beam energy of 2.4 GeV, we can deduce that an undulator period λ_w = 1.2 cm, corresponding to a peak on-axis magnetic field of $B = 0.93$ T, is suitable for emitting at 3 keV. Both the structure and length of the undulator depend on the seeding scheme: the XFELO requires a single short undulator module, equipped with a sequence of X-ray crystal mirrors.

Table 1. Electron beam for MariX FEL.

Property	Unit	Value	Property	Unit	Value
Energy	GeV	1.6–3.8	Current	kA	1.6
Charge	pC	8–50	Bunch duration	fs	2.5–16
rms relative energy spread	10^{-4}	5–3	slice energy spread	10^{-4}	4–2
rms normalized emittance	mm mrad	0.3–0.5	slice normalized emittance	mm mrad	0.3–0.5

FEL simulations have been performed with the three-dimensional code GENESIS 1.3 [53] in time-dependent mode. The SASE radiation at 4.16 Angstrom is described for reference in Figure 1.

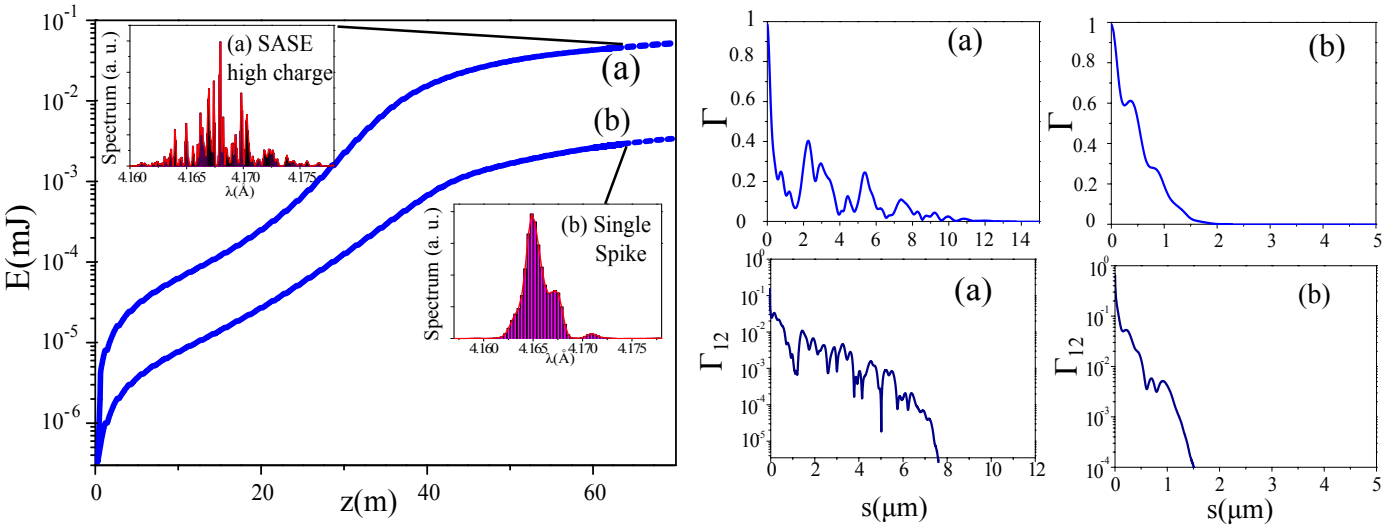

Figure 1. Left plot: SASE energy growth for the high (**a**) and low (**b**) charge working points and corresponding spectral profiles at saturation (inner boxes). **Right windows**: self (Γ, upper row) and mutual ($\Gamma_{1,2}$, lower row) coherence degrees vs. $s = c\tau$ for the two analyzed working points (**a**) and (**b**).

On the left, the growth along the undulator is presented for (a) high (50 pC) and (b) low (8 pC) charge cases. Saturation is reached in about 50 m with a level of (a) 8×10^{11} and (b) 4×10^9 photons/pulse, respectively. The spectral profiles are reported in the inner boxes, showing the SASE fluctuations in the high charge case (a) and the single spike mode in the low charge one (b). The coherence degree, evaluated from the correlation,

$$\Gamma_{n,m}(\tau) = \left| \frac{\int dt E_n(t) E_m(t-\tau)}{\sqrt{\int dt |E_n|^2} \sqrt{\int dt |E_m|^2}} \right|, \quad (2)$$

between two different generic pulses or for one single pulse ($\Gamma = \Gamma_{1,1}$), is shown in the windows on the right part of Figure 1. In expression (2), E_n and E_m are the complex electric fields of the pulses as a function of time. In the SASE mode (case (a)), phase coherence on one single pulse and shot-to-shot stability are poor, with a coherence length less than 1 μm over a 10 μm long pulse and an equal time coherence degree ($\Gamma_{1,2}(0)$) of about 4×10^2. In the single spike mode (case (b)), the coherence length coincides with the pulse's, but the shot-to-shot stability is low, with $\Gamma_{1,2}(0) = 2 \times 10^1$. The characteristics of the SASE radiation are summarized in Table 2, in the third (high charge working point) and fourth (single spike mode) columns. The patterns of the SASE power (a) and spectral distribution (b) are shown in Figure 2 as a function of the number of shots. From this graph, the modest size of the coherence areas and the poor stability of the SASE process are evident.

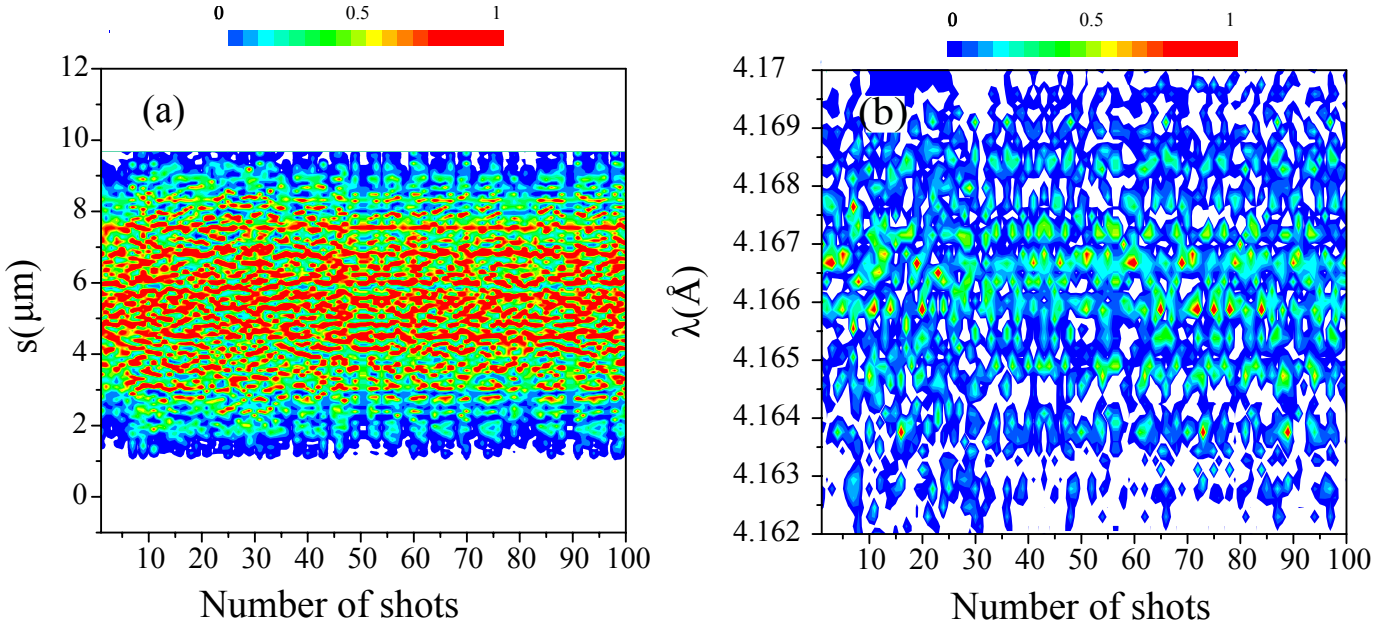

Figure 2. SASE (**a**) power vs. $s = c\tau$ and (**b**) spectrum vs. λ as a function of the number of shots. Logarithmic scale.

The XFELO operation has been numerically studied by extracting the radiation simulated by GENESIS 1.3 from the oscillator undulator, driving it through the optical line and superimposing it on the successive electron bunches. In order to simulate the electron bunch train fluctuations, the microscopic distribution of the electron beam is changed shot-to-shot in the simulations. The transport inside the cavity is done by using the Huygens integral [54]

$$E(\underline{x}', t') = \frac{i}{B\lambda_0} \int d\underline{x} E(\underline{x}, t) e^{-\frac{i\pi}{\lambda B}(Ar^2 - 2(xx' + yy) + Dr'^2)}, \quad (3)$$

where $\underline{x} = (x; y)$, $r^2 = x^2 + y^2$ and $r'^2 = x'^2 + y'^2$. Here, the electric field is the output of the FEL simulation (performed with about 2048 particles and 7000 slices), which is extracted at the end of the undulator over a three-dimensional grid (grid dimensions: transverse ~ 2 μm, longitudinal ~ 1.6 nm). In the first step, the Huygens integral is extended from the end of the undulator up to the first mirror. A, B, C and D are the elements of a 2×2 matrix describing the optical path and depending on the drift length and on the focal length of the mirror. The effect of the mirror is modelled with a transfer function, taking into account its

reflectivity and spectral selectivity. Its action is evaluated by computing the convolution between the electric field at the mirror position and the Fourier anti-transform T of the mirror transfer function,

$$E(\underline{x}, t') = \frac{1}{\sqrt{2\pi}} \int dt T(t - t') E(\underline{x}, t). \quad (4)$$

The process is reiterated for each drift and cavity mirror up to the beginning of the undulator in the next step. The electric field, calculated in this way, is superimposed to the successive electron bunches after each cavity round trip. The mirror and beam splitter reflectivities have been simulated with the XOP (X-ray Oriented Programs) code [55].

3. Results

Figure 3 shows the scheme of the coherent source, constituted by a short (about 7–10 m long) undulator module with period λ_w = 1.2 cm, embedded within a ring cavity.

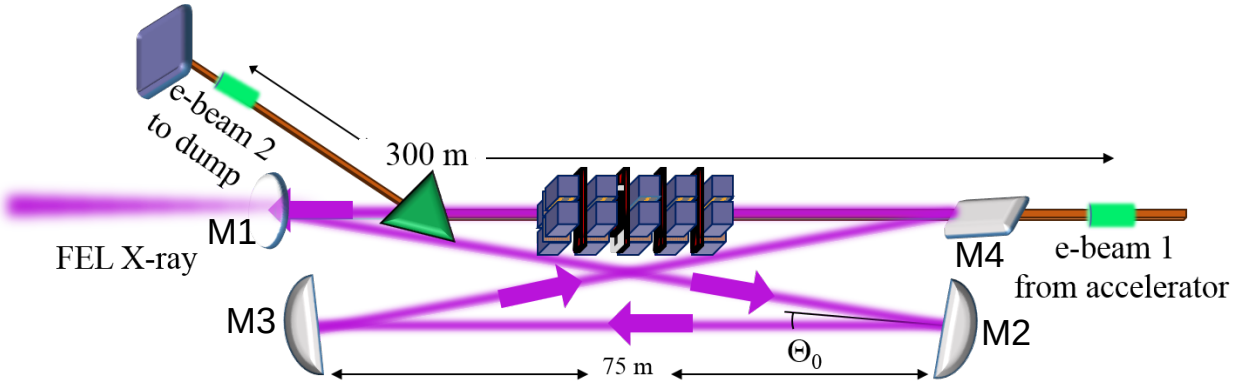

Figure 3. Scheme of the X-ray FEL Oscillator: λ_w = 1.2 cm undulator module within a ring cavity made of three Diamond mirrors (M_2, M_3 and M_4) and one beam splitter (M_1, outcoupling the radiation). The X-ray radiation is emitted from right to left. Θ_0 is the incidence angle on the cavity mirrors with respect to the normal. The distance $M_{1,4}$–$M_{3,2}$ between two mirrors is 75 m, giving a cavity round trip length of 300 m, equal to the distance between two successive electron bunches.

For an electron beam repetition rate of 1 MHz, the round trip of the cavity must be 300 m. The sequence of the accelerated beam packets entering the undulator is synchronized with the radiation reflected and recirculated by hard X-ray mirrors. Three Diamond mirrors and one beam splitter, made by Zincblend perfect single crystals (lattice parameters: $a = b = c$ = 3.566 Å, $\alpha = \beta = \gamma$ = 90) operating in the range of about 3.0–3.5 keV, namely 3.6–4 Å(with an incidence angle θ < 30 from normal), have been considered. At least two of the mirrors are assumed to be bent and focusing.

Figure 4 presents the transfer function T of the total optical line as a function of the energy of the photons for a central energy of 3.015 keV and a quasi-orthogonal reflection (incidence angle Θ_0 = 3), compared with the natural SASE spectral line.

The mirror transfer function is narrower than the natural FEL spectral line and the spectral filtering of the mirrors is the dominant effect in the reduction of the spectral width. The angular filtering is instead absolutely inefficient, since the angular width of the transfer function is about 2 mrad, to be compared to the much smaller SASE divergence of 25 μrad. FEL simulations were performed for a 50 pC electron beam. Figure 5 shows the intracavity radiation energy as a function of the number of round trips. The saturation is reached in about 50 cycles, with an intracavity energy level of about 20 μJ. Due to the short undulator and wavelength, the slippage is very low: the simulated time window (12 μm) is thus adjusted to the electron beam and reported in the inner boxes of Figure 5.

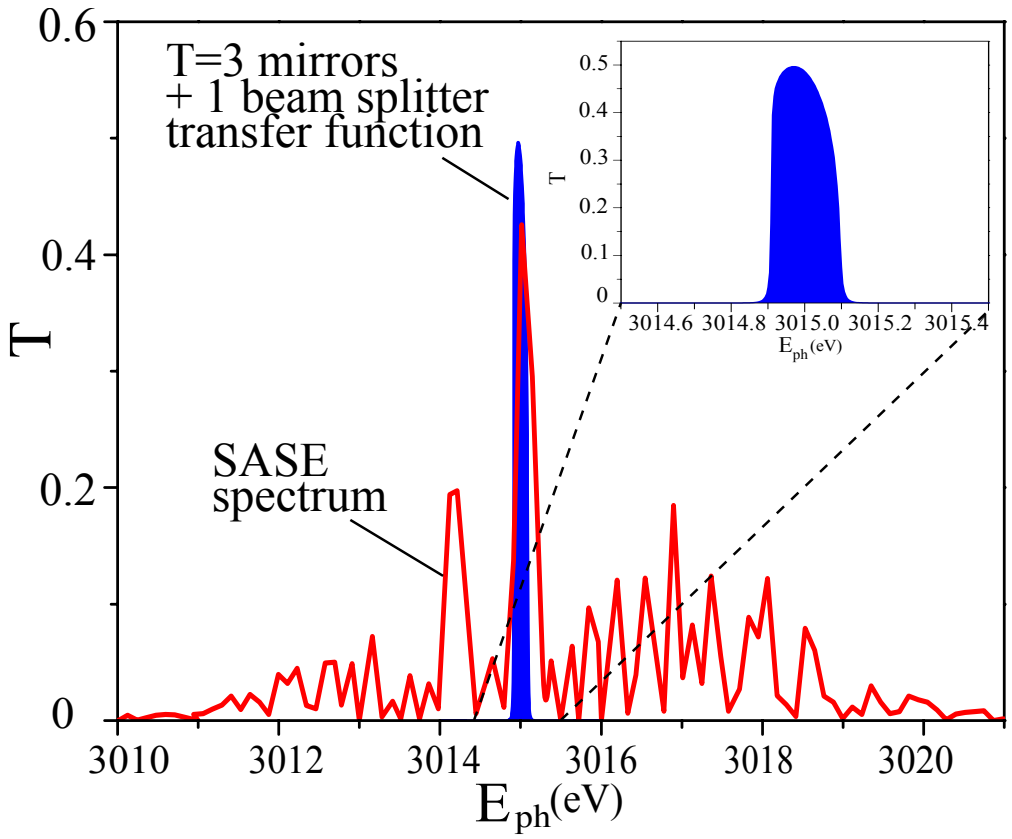

Figure 4. Transfer function T of an optical line made by three diamond mirrors and one beam splitter (in blue) vs. the photon energy for an incidence angle Θ_0 of 3 with respect to the normal. SASE spectrum (in red) in arbitrary units. The reflectivities are simulated with the XOP code [55].

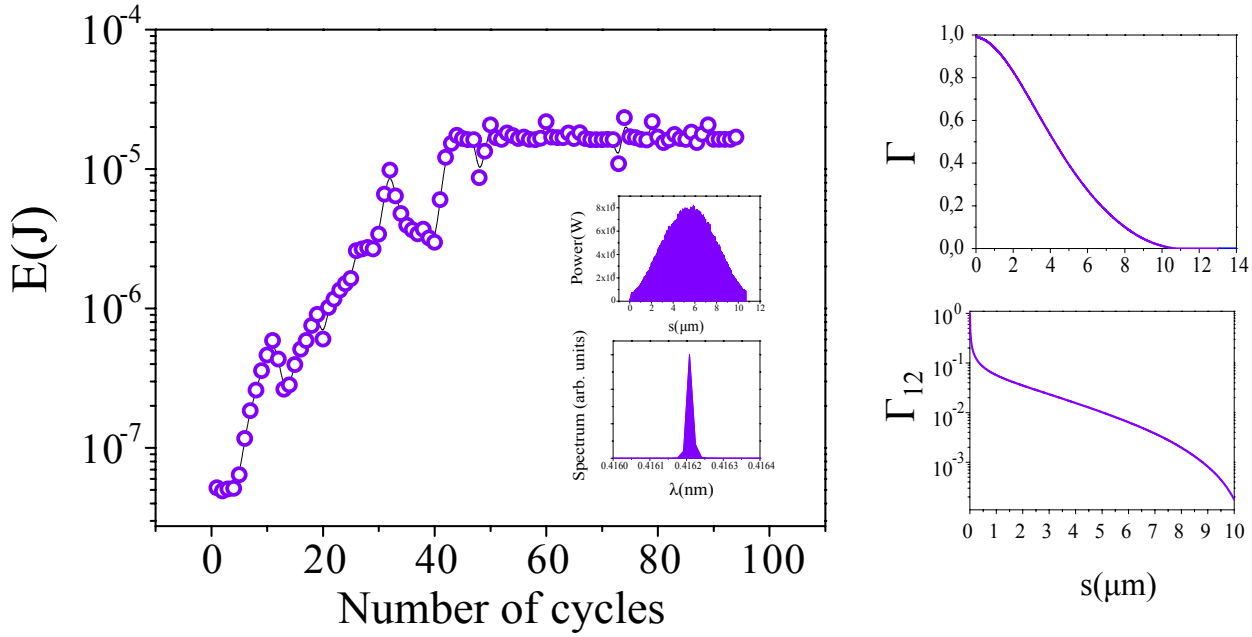

Figure 5. FEL Oscillator. **Left window**: intracavity energy growth as a function of the number of round trips. Inner boxes: temporal and spectral distributions at saturation. **Right windows:** auto (Γ) and mutual ($\Gamma_{1,2}$) coherence degrees vs. $s = c\tau$.

Jitters occur due to the different microscopic structures of the successive electron bunches. In the inner boxes, the temporal and spectral distributions at saturation are

presented. The right windows of Figure 5 show the auto (Γ) and mutual ($\Gamma_{1,2}$) coherence degrees of the XFEL-Oscillator, pointing out its enhanced coherence and stability with respect to the SASE's reported in Figure 1.

The longitudinal distributions along $s = c\tau$ of the power (a) and the spectral amplitude structure (b) are shown in Figure 6 as a function of the round trip number in the X-ray cavity. The output radiation is much more stable and quasi monochromatic if compared to the analogous patterns of the SASE radiation already shown in Figure 2. The studied X-FEL Oscillator results in an almost fully coherent pulse, characterized by a very small spectral bandwidth. Table 2 summarizes the main properties of SASE (third and fourth columns) and XFELO (fifth column) radiation. Despite the lower number of photons produced by the XFELO with respect to the SASE case, its pulses' stability, directionality and brilliance are higher.

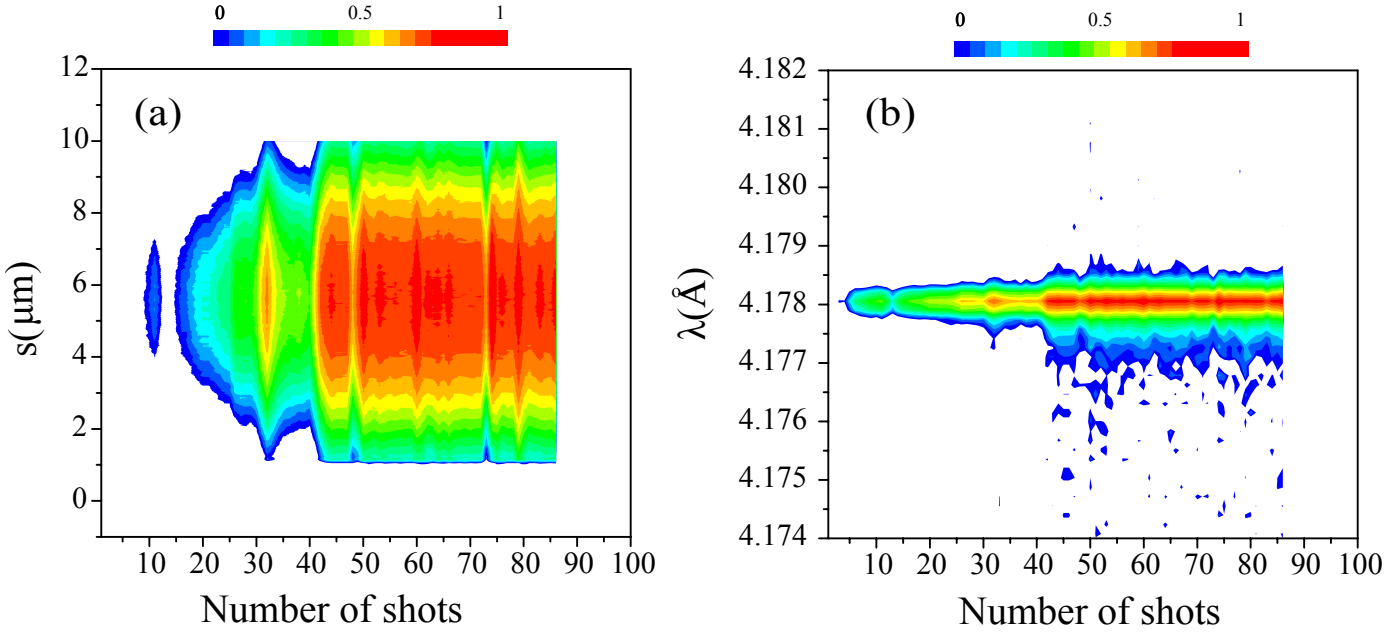

Figure 6. Intracavity power vs. s and spectrum vs. λ as a function of the round trip number in logarithmic scale. XFELO (**a**) intra-cavity power vs $s = c\tau$ and (**b**) spectrum vs λ as function of the round trip number. Logarithmic scale.

Table 2. The repetition rate of the source is 1 MHz. $=Photons/s/mm^2/mrad^2/bw(‰).

Radiation Mode		**SASE**	**Single Spike**	**XFELO**
Electron charge	pC	50	8	50
Photon energy	keV	3	3	3
Radiation wavelength	Å	4.16	4.16	4.16
Photon/shot	10^{10}	80	0.36	4.4
Bandwidth	0.1%	2.1	0.7	4
Pulse length	fs	10	3	16
Pulse divergence	μrad	25	45	14
Pulse size	μm	130	140	35
Radiation energy	μJ	55	1.7	21
Photon/s	10^{16}	80	0.36	4.4
Peak brilliance	$10^{30}$$	3.6	0.043	3.8
Average brilliance	$10^{22}$$	3.6	0.013	4

4. Conclusions

The MariX facility is dedicated to and optimized for ultrafast coherent-X-ray spectroscopy and inelastic photon scattering, and for highly penetrating X-ray imaging of mesoscopic and macroscopic samples. In the range of wavelengths between 2 and 5 Å, MariX provides 10^{10}–10^{11} photons per shot with a repetition rate of 1 MHz in SASE mode. The studied X-ray FEL Oscillator configuration based on diamond mirrors produces 10^{7}–10^{10} coherent photons per shot at 3–3.5 keV at 1 MHz. These estimations do not take into account degradations due to errors, misalignments or jitters, and exceed by one or more orders of magnitude the target values set by the scientific case. MariX will therefore be capable of satisfying the expected FEL photon beam parameters, considering also a safety margin dealing with the losses in delivering the photon beams to the experimental hutch. Higher repetition rates could relax the cavity length requirements. The novel source will create absolutely novel conditions for experiments that cannot be performed satisfactorily at the present and foreseen sources based on storage rings or SASE-FEL.

Author Contributions: Conceptualization V.P., L.S., A.T. and M.O.; Definition of the scientific case G.R.; Methodology V.P., M.O., A.T.; Software and data curation M.O., M.R.C. and A.B.; Writing—original draft preparation V.P. and M.O.; writing—review and editing V.P., M.O.; Supervision V.P., L.S. and G.R.; Funding acquisition A.R.R., L.S. All authors have read and agreed to the published version of the manuscript.

Funding: This research received no external funding.

Institutional Review Board Statement: Not applicable.

Informed Consent Statement: Not applicable.

Conflicts of Interest: The authors declare no conflict of interest.

References

1. Faatz, B.; Schreiber, S. First Lasing of FLASH2 at DESY Synch. *Rad. News* **2014**, *27*, 6.
2. Emma, P.; Akre, R.; Arthur, J.; Bionta, R.; Bostedt, C.; Bozek, J.; Brachmann, A.; Bucksbaum, P.; Coffee, R.; Decker, F.-J.; et al. First lasing and operation of an Angstrom-wavelength free-electron laser. *Nat. Phot.* **2010**, *4*, 641. [CrossRef]
3. Pile, D. First light from SACLA. *Nat. Phot.* **2011**, *5*, 456. [CrossRef]
4. Weise, H.; Decking, W. Commissioning and First Lasing of the European XFEL. In Proceedings of the FEL2017, MOC03, Santa Fe, NM, USA, 20–25 August 2017.
5. Gruenbein, M.L.; Bielecki, J.; Gorel; A.; Stricker, M.; Bean, R.; Cammarata, M.; Doerner, K.; Froehlich, L.; Hartmann, E. Megahertz data collection from protein microcrystals at an X-ray free-electron laser. *Nat. Comm.* **2018**, *9*, 3487. [CrossRef]
6. SwissFEL at Paul Scherrer Institute (PSI) Website. Available online: https://www.psi.ch/en/swissfel/about-swissfel (accessed on 1 June 2021).
7. Ko, I.S.; Kang, H.; Heo, H.; Kim, C.; Kim, G.; Min, C.K.; Yang, H.; Baek, S.Y.; Choi, H.; Mun, G.; et al. Construction and commissioning of PAL-XFEL facility. *Appl. Sci.* **2017**, *7*, 479. [CrossRef]
8. Wang, D.; SXFEL team. Soft X-ray Free-Electron Laser at SINAP. In Proceedings of the IPAC2016, TUZA01, Busan, Korea, 8–13 May 2016.
9. Allaria, E.; Appio, R.; Badano, L.; Barletta, W.A.; Bassanese, S.; Biedron, S.G.; Borga, A.; Busetto, E.; Castronovo, D.; Cinquegrana, P.; et al. Highly coherent and stable pulses from the FERMI seeded free-electron laser in the extreme ultraviolet. *Nat. Phot.* **2012**, *6*, 699. [CrossRef]
10. Giannessi, L.; Artioli, M.; Bellaveglia, M.; Briquez, F.; Chiadroni, E.; Cianchi, A.; Couprie, M.E.; Dattoli, G.; Di Palma, E.; Di Pirro, G.; et al. High-Order-Harmonic Generation and Superradiance in a Seeded Free-Electron Laser. *Phys. Rev. Lett.* **2012**, *108*, 164801. [CrossRef] [PubMed]
11. Yu, L.H.; Babzien, M.; Ben-Zvi, I.; DiMauro, L.F.; Doyuran, A.; Graves,W.; Johnson, E.; Krinsky, S.; Malone, R.; Pogorelsky, I.; et al. High-gain harmonic-generation free-electron laser. *Science* **2000**, *289*, 932. [CrossRef]
12. Doyuran, A.; Di Mauro, L.; Graves, W.S.; Johnson, E.D.; Heese, R.; Krinsky, S.; Loos, H. Characterization of a high-gain harmonic-generation free-electron laser at saturation. *Phys. Rev. Lett.* **2001**, *86*, 5902. [CrossRef] [PubMed]
13. Takahashi, E.J.; Nabekawa, Y.; Mashiko, H.; Hasegawa, H.; Suda, A.; Midorikawa, K. Generation of strong optical field in soft X-ray region by using high-order harmonics. *IEEE J. Quant. Electr.* **2004**, *10*, 6. [CrossRef]
14. Yu, L.H.; DiMauro, L.; Doyuran, A.; Graves,W.S.; Johnson, E.D.; Heese, R.; Krinsky, S.; Loos, H.; Murphy, J.B.; Rakowsky, G.; et al. First Ultraviolet High-Gain Harmonic-Generation Free-Electron Laser. *Phys. Rev. Lett.* **2003**, *91*, 074801. [CrossRef]

15. Togashi, T.; Takahashi, E.J.; Midorikawa, K.; Aoyama, M.; Yamakawa, K.; Sato; T.; Iwasaki, A.; Owada, S.; Yamanouchi, K.; Hara, T. Extreme ultraviolet free electron laser seeded with high-order harmonic of Ti:sapphire laser. *Opt. Exp.* **2011**, *19*, 317 . [CrossRef] [PubMed]
16. Giannessi, L.; Bellaveglia, M.; Chiadroni, E.; Cianchi, A.; Couprie, M.E.; DelFranco, M.; Di Pirro, G.; Ferrario, M.; Gatti, G.; Labat, M.; et al. Superradiant Cascade in a Seeded Free-Electron Laser. *Phys. Rev. Lett.* **2013**, *110*, 04480. [CrossRef]
17. Xiang, D.; Stupakov, G. Echo-enabled harmonic generation free electron laser. *Phys. Rev. Accel. Beams* **2009**, *12*, 030702. [CrossRef]
18. Hemsing, E.; Dunning, M.; Garcia, B.; Hast, C.; Raubenheimer, T.; Stupakov, G.; Xiang, D. Echo- enabled harmonics up to the 75th order from precisely tailored electron beams. *Nat. Phot.* **2016**, *10*, 512. [CrossRef]
19. Feng, C.; Deng, H.; Zhang, M.; Wang, X.; Chen, S.; Liu, T.; Zhou, K.; Gu, D.; Wang, Z.; Jiang, Z.; et al. Coherent extreme ultraviolet free-electron laser with echo-enabled harmonic generation. *Phys. Rev. Accel. Beams* **2019**, *22*, 050703. [CrossRef]
20. Rebernik Ribič, P.; Abrami, A.; Badano, L.; Bossi, M.; Braun, H.H.; Bruchon, N.; Capotondi, F.; Castronovo, D.; Cautero, M.; Cinquegrana, P.; et al. Coherent soft X-ray pulses from an echo-enabled harmonic generation free-electron laser nature research. *Nat. Phot.* **2019**, *13*, 1–7. [CrossRef]
21. Lambert, G.; Gautier, J.; Hauri, C.P.; Zeitoun, P.; Valentin, C.; Marchenko, T.; Tissandier, F.; Goddet, J.P.; Ribière, M.; Rey, G.; et al. An optimized kHz two-colour high harmonic source for seeding free-electron lasers and plasma-based soft X-ray lasers. *New J. Phys.* **2009**, *11*, 083033. [CrossRef]
22. Labat, M.; Bellaveglia, M.; Bougeard, M.; Carré, B.; Ciocci, F.; Chiadroni, E.; Cianchi, A.; Couprie, M.E.; Cultrera, L.; Del Franco, M.; et al. High-Gain Harmonic-Generation Free-Electron Laser Seeded by Harmonics Generated in Gas. *Phys. Rev. Lett.* **2011**, *107*, 224801. [CrossRef] [PubMed]
23. Petrillo, V.; Opromolla, M.; Bacci, A.; Drebot, I.; Ghiringhelli, G.; Petralia, A.; Puppin. E.; Rossetti Conti, M.; Rossi, A.R.; Tagliaferri, A.; et al. High repetition rate and coherent Free-Electron Laser in the X-rays range tailored for linear spectroscopy. *Instruments* **2019**, *3*, 47. [CrossRef]
24. Wurtele, J.; Gandhi, P.; Gu, W.X. Tunable soft X-ray oscillators. In Proceedings of the FEL2010, Malmö, Sweden, 23–27 August 2010.
25. Petrillo, V.; Opromolla, M.; Bacci, A.; Broggi, F.; Drebot, I.; Ghiringhelli, G.; Puppin, E.; Rossetti Conti, M.; Rossi, A.R.; Ruijter, M.; et al. Coherent, high repetition rate tender X-ray Free-Electron Laser seeded by an Extreme Ultra-Violet Free-Electron Laser Oscillator. *New J. Phys.* **2020**, *22*, 073058. [CrossRef]
26. Mirian, N.S.; Opromolla, M.; Rossi, G.; Serafini, L.; Petrillo, V. High repetition rate and coherent Free-Electron Laser in the tender X-rays based on the Echo-Enabled Harmonic Generation of an Ultra-Violet Oscillator pulse. *Phys. Rev. Accel. Beams* **2021**, *24*, 050702. [CrossRef]
27. Ackermann, S.; Faatz, B.; Grattoni, V.; Kazemi, M.-M.; Lang, T.; Leclmer, C.; Paraskaki, G.; Zemella, J. Novel method for the generation of stable radiation from free-electron lasers at high repetition rates. *Phys. Rev. Accel. Beams* **2020**, *23*, 071302. [CrossRef]
28. Rosenzweig, J.; Alesini, D.; Andonian, G.; Boscolo, M.; Dunning, M.; Faillace, L.; Ferrario, M.; Fukusawa, A.; Giannessi, L. Generation of ultra-short, high brightness electron beams for single-spike SAS FEL operation. *Nucl. Instr. Meth. Phys. Res. Sect. A* **2008**, *593*, 39. [CrossRef]
29. Marinelli, A.; MacArthur, J.; Emma, P.; Guetg, M.; Field, C.; Kharakh, D.; Lutman, A.A.; Ding, Y.; Huang, Z. Experimental demonstration of a single-spike hard-X-ray free-electron laser starting from noise. *Appl. Phys. Lett.* **2017**, *111*, 151101. [CrossRef]
30. Villa, F.; Anania, M.P.; Artioli, M.; Bacci, A.; Bellaveglia, M.; Bisesto, M.G.; Biagioni, A.; Carpanese, M.; Cardelli, F.; Castorin, G. Generation and characterization of ultra-short electron beams for single spike infrared FEL radiation at SPARC_LAB. *Nucl. Instr. Meth. Phys. Res. Sect. A* **2017**, *865*, 43–46. [CrossRef]
31. Geloni, G.; Kocharyan, V.; Saldin, E. '=A novel self-seeding scheme for hard X-ray FELs. *J. Mod. Opt.* **2011**, *58*, 1391–1403. [CrossRef]
32. Amann, J.; Berg, W.; Blank, V.; Decker, F.-J.; Ding, Y.; Emma, P.; Feng, Y.; Frisch, J.; Fritz, D.; Hastings, J.; et al. Demonstration of self-seeding in a hard-X-ray free-electron laser. *Nat. Phot.* **2012**, *6*, 693–698. [CrossRef]
33. Dattoli, G.; Palma, E.D.; Petralia, A. Free-electron laser oscillator efficiency. *Opt. Comm.* **2018**, *425*, 29.
34. Ciocci, F.; Dattoli, G.; De Angelis, A.; Faatz, B.; Garosi, F.; Giannessi, L.; Ottaviani, P.L.; Torre, A. Design considerations on a high-power VUV FEL. *IEEE J. Quant. Electr.* **1995**, *31*, 1242–1252. [CrossRef]
35. der Slot, P.J.M.V.; Freund, H.P.; Miner, W.W., Jr.; Benson, S.V.; Schinn, M.; Boller K.-J. Time-dependent Three dimensional simulation of free-electron laser oscillators. *Phys. Rev. Lett.* 2009, 102, 244802. [CrossRef] [PubMed]
36. Kim, K.-J.; Shvyd'ko, Y. Tunable optical cavity for an X-ray Free-Electron Laser Oscillator. *Phys. Rev. Accel. Beams* **2009**, *12*, 030703. [CrossRef]
37. Kim, K.-J.; Shvyd'ko, Y.; Reiche, S. A proposal for an X-ray oscillator with an Energy recovery Linac. *Phys. Rev. Lett.* **2008**, *100*, 244802. [CrossRef]
38. Shvyd'ko, Y.; Stoupin, S.; Cunsolo, A.; Said, A.H.; Huang, X. High-reflectivity high-resolution X-ray crystal optics with diamonds. *Nat. Phys.* **2010**, *6*, 196. [CrossRef]
39. Qin, W.; Huang, S.; Liu, K.X.; Kim, K.-J.; Lindberg, R.R.; Ding, Y.; Huang, Z.; Maxwell, T.; Bane, K.; Marcus, G. Start-to-end simulations for an X-ray FEL oscillator at the LCLS-II and LCLS-HE. In Proceedings of the FEL2017, Santa Fe, NM, USA, 20–25 August 2017.

40. Huang, Z.; Ruth, R.D. Fully Coherent X-Ray Pulses from a Regenerative-Amplifier Free-Electron Laser. *Phys. Rev. Lett.* **2006**, *96*, 144801. [CrossRef]
41. McNeil, B.W.J.; Thompson, N.R.; Dunning, D.J.; Karssenberg, J.G.; van der Slot, P.J.M.; Boller, K.-J. A design for the generation of temporaly-coherent radiation pulses in the VUV and beyond by a seld-seeded high gain free electron laser amplifier. *New J. Phys.* **2007**, *9*, 239. [CrossRef]
42. Li, K.; Deng, H. Systematic design and three-dimensional simulation of X-ray FEL oscillator for Shanghai Coherent Light Facility. *Nucl. Instr. Meth. Phys. Res. Sect. A* **2018**, *895*, 40–47. [CrossRef]
43. Marcus, G.; Ding, Y.; Feng, Y.; Halavanau, A.; Huang, Z.; Krzywinski, J.; MacArthur, J.; Margraf, R.; Raubenheimer T.; Zhu, D.; et al. Regenerative amplification for a hard-X ray Free-Electron laser. In Proceedings of the FEL 2019, TUP032, Hamburg, Germany, 26–30 August 2019.
44. Marcus, G.; Decker, F.-J. Cavity-based Free-Electron Laser research and development: A Joint Argonne National Laboratory and SLAC National Laboratory collaboration. In Proceedings of the FEL 2019, TUD04, Hamburg, Germany, 6–30 August 2 2019.
45. Freund, H.P. ; Slot, P.J.M.v.; Shvydko, Y. An X-ray Regenerative Amplifier Free-Electron Laser Using Diamond Pinhole Mirrors. *New J. Phys.* **2019**, *21*, 093028. [CrossRef]
46. Li, A.K.; Yan, J.; Feng, C.; Zhang, M.; Deng, H. High brightness fully coherent X-ray amplifier seeded by a free-electron laser oscillator. *Phys. Rev. Accel. Beams* **2018**, *21*, 040702. [CrossRef]
47. Freund, H.P.; Nguyen, D.C.; Sprangle, P.A.; Slot, P.J.M.V. Three-dimensional, time-dependent simulation of a regenerative amplifier free-electron laser. *Phys. Rev. Accel. Beams* **2013**, *16*, 010707. [CrossRef]
48. Serafini, L.; Bacci, A.; Bellandi, A.: Bertucci, M.; Bolognesi, M.; Bosotti, A.; Broggi, F.; Calandrino, R.; Camera, F.; Canella, F.; et al. MariX, an advancedMHz-class repetition rate X-ray source for linear regime time-resolved spectroscopy and photon scattering. *Nucl. Instr. Meth. Phys. Res. Sect. A* **2019**, *930*, 167–172. [CrossRef]
49. Mitri, S.D.; Cornacchia, M. Transverse emittance-preserving arc compressor for highbrightness electron beam-based light sources and colliders. *Europhys. Lett.* **2015**, *109*, 62002. [CrossRef]
50. Mitri, S.D. Feasibility study of a periodic arc compressor in the presence of coherent synchrotron radiation. *Nucl. Instr. Meth. Phys. Res. Sect. A* **2016**, *806*, 184. [CrossRef]
51. Placidi, M.; Di Mitri, S.; Pellegrini, C.; Penn, G. Compact FEL-driven inverse compton scattering gamma-ray source. *Nucl. Instr. Meth. Phys. Res. Sect. A* **2017**, *855*, 55–60. [CrossRef]
52. Bacci, A.; Rossetti Conti, M.; Bosotti, A.; Cialdi, S.; Di Mitri, S.; Drebot, I.; Faillace, L.; Ghiringhelli, G.; Michelato, P.; Monaco, L.; et al. Two-pass two-way acceleration in a Super-Conducting CW linac to drive low jitters X-ray FELs. *Phys. Rev. Accel. Beams* **2019**, *22*, 111304. [CrossRef]
53. Reiche, S. GENESIS 1.3: A fully 3D time-dependent FEL simulation code. *Nucl. Instr. Meth. Phys. Res. Sect. A* **1999**, *429*, 243. [CrossRef]
54. Belanger, P.A. Beam propagation and the ABCD ray matrices. *Opt. Lett.* **1991**, *16*, 196. [CrossRef] [PubMed]
55. Software XOP, Download from European Synchrotron Radiation Facility Website. Available online: https://www.esrf.fr/Instrumentation/software/data-analysis/xop2.4 (accessed on 1 May 2020).